Pharmaceutical Research, Vol. 25, No. 2, February 2008 (© 2007)
DOI: 10.1007/s11095-007-9483-1

Research Paper

Effects of Vial Packing Density on Drying Rate during Freeze-drying of Carbohydrates or a Model Protein Measured using a Vial-weighing Technique

Henning Gieseler[1] and Geoffrey Lee[1,2]

Received July 20, 2007; accepted October 17, 2007; published online November 13, 2007

Purpose. To determine the effects of vial packing density in a laboratory freeze dryer on drying rate profiles of crystalline and amorphous formulations.
Methods. The Christ freeze-drying balance measured cumulative water loss, $m(t)$, and instantaneous drying rate, $\dot{m}(t)$, of water, mannitol, sucrose and sucrose/BSA formulations in commercial vials.
Results. Crystalline mannitol shows drying rate behaviour indicative of a largely homogeneous dried-product layer. The drying rate behaviour of amorphous sucrose indicates structural heterogeneity, postulated to come from shrinkage or microcollapse. Trehalose dries more slowly than sucrose. Addition of BSA to either disaccharide decreases primary drying time. Higher vial packing density greatly reduces drying rate because of effects of radiation heat transfer from chamber walls to test vial.
Conclusions. Plots of $m(t)$ *versus* $\sqrt{t}$ and $\dot{m}(t)$ *versus* layer thickness (either ice or dried-product) allow interpretation of changes in internal cake morphology during drying. Vial packing density greatly influences these profiles.

KEY WORDS: drying rate; freeze-drying; product morphology; product resistance.

INTRODUCTION

During the primary (1°) drying step of the freeze-drying process the product temperature, T_p, at a given shelf temperature, chamber pressure and type of vial is determined by the dry-product layer resistance, $R_p(t)$. A high resistance leads to a high T_p, and vice versa. The T_p of a formulation with low $R_p(t)$ is more sensitive to chamber pressure than to shelf temperature, whereas the T_p of a formulation with high $R_p(t)$ is more dependent on shelf temperature. The behaviour of $R_p(t)$ during 1° drying can reveal useful information about structural changes occurring in the product, e.g. micro-collapse, cracking of the cake, formation of a high resistance surface, etc. As a consequence, $R_p(t)$ is currently being discussed within the PAT initiative as one of the most important product-related critical process parameter (CPP) in a freeze-drying operation.

The CWS-40 freeze-drying balance is a research tool that stands on a shelf in the drying chamber of a freeze-dryer and weighs a single vial. It has been used to delineate mass flux with different freezing protocols or shelf temperatures and chamber pressures during 1° drying (1). Although the balance monitors but a single vial, its strength lies in a direct determination of the instantaneous drying-rate, $\dot{m}(t)$, of a given formulation in the vial at any time during 1° drying. The $\dot{m}(t)$ is inversely related to $R_p(t)$. A previous study (2) utilised a single vial placed in the centre of one shelf in an otherwise empty drying chamber. It is known, however, that both the total vial load and the geometry of the vial packing on a shelf in a freeze-dryer chamber has substantial affects on heat and mass transfer during 1° drying (3). A valid analysis of $\dot{m}(t)$ data obtained with a partial vial load in the drying chamber requires, however, knowledge of the impact of shelf vial loading on $\dot{m}(t)$ provided by the balance. This allows prediction of the drying conditions suitable for a full vial load. Indeed, the ramifications of the expected strong influence of vial load on $\dot{m}(t)$are of substantial interest to development freeze-drying studies under partial load conditions.

When the number of vials increases, then the total amount of ice to be removed is greater, but the heat transfer rate available to the vials, $\dot{Q}(t)$, remains the same (4):

$$\dot{Q}(t) = A_v \cdot K_v(T_s - T_p) = \Delta H_s \dot{m}(t) \quad (1)$$

where A_v is the external cross-sectional area of the vial (cm) available for heat transfer, K_v is the heat transfer coefficient (cal s^{-1} cm^{-2} K^{-1}), T_S is the temperature of the shelf (°C), and ΔH_s is the latent heat of sublimation. The total number of vials placed on a shelf will have an impact on the average K_v obtained for these vials. The common procedure used to

[1] Division of Pharmaceutics, Friedrich-Alexander-University, Cauerstr. 4, 91058, Erlangen, Germany.
[2] To whom correspondence should be addressed. (e–mail:lee@pharmtech.uni-erlangen.de)

evaluate K_v is to perform sublimation tests with pure water under steady state conditions (5). Pikal (6) recognised that:

$$Kv = Kc + Kr + Kg \quad (2)$$

where K_c denotes heat conduction to the product from the shelf through the vial/shelf contact points, K_r denotes radiation from the top and bottom shelves as well as from the chamber walls/door, and K_g denotes 'convective' (mostly free-molecular flow and only partly bulk fluid flow) heat transfer from the bottom shelf via the gas located between the vial base and the shelf. An increase in the total vial load on a shelf is expected to reduce K_v because of a reduction in the contribution of K_r (mainly from the chamber walls and the chamber door) to Eq. 2. With a large vial load the proportion of 'edge' vials (running at a higher average T_p than fully-shielded vials) relative to 'centre' vials (running at lower T_p) decreases. According to Eq. 1 $\dot{m}(t)$ should therefore decrease as the total vial number increases.

This paper presents our efforts to determine quantitatively the effects of vial load in a laboratory-scale freeze-dryer on the drying-rate results obtained from the freeze-drying balance. Previous direct measurements of sublimation rate during freeze-drying utilised, for example, a filled-capillary (7) and not a vial, or were restricted to single weighings at the beginning and end of 1° drying (3). The balance provides an instantaneous drying-rate measurement of a given formulation contained in a commercial serum-tubing vial (2–20 mL). First, the drying-rate profiles of water were determined in dependence of vial packing density, and the results plotted as $\dot{m}(t)$*versus* residual ice layer thickness and analysed. Secondly, the effects of vial packing density on the drying rate profiles of aqueous solutions of the crystalline bulking agent mannitol, amorphous stabilizers, sucrose and trehalose, or the model protein, BSA, were examined. The changes in $\dot{m}(t)$ with increasing dried-product layer thickness are given and an attempt made to relate this to likely changes occurring in the internal morphology cake during 1° drying. Finally, an integrated drying time is determined from each drying-rate profile to quantify the duration of 1° drying. This study demonstrates further the utility of the balance as a research and development tool that is particularly useful when only small amounts of product (e.g. an expensive protein) are available.

MATERIALS AND METHODS

Materials

Sucrose, trehalose dihydrate, mannitol and bovine serum albumin (BSA) were all obtained from Sigma Chemicals (D-Munich) and used as received. Water was double-distilled from an all-glass apparatus.

Freeze-drying Balance

A balance model CWS-40, 2000 (second edition) was used for his work (Christ, D-Osterode). The balance and its operation have been fully described before (1). This newer version is an improved model that has better electro-mechanical force compensation, improved hydraulic oil allowing better performance <−30°C, and a new design of the lifting arm. Additionally, the measurement range has been extended to 0.005–50 g. The system was calibrated monthly using the balance software with external weights of 50 g, 1 g and 10 mg. An offset alignment was performed before each run throughout the study. 10 mL glass vials were used of internal cross-sectional area (A_p) 3.63 cm^2 and external cross-sectional area (A_v) 4.52 cm^2. A user-defined weighing interval of 10 min was used throughout this work.

Freeze-drying Procedure

2.5 g of each solvent or solution (w/w) to be investigated was filtered through a 0.22 μm membrane filter (Milex-GV, Millipore) directly into a vial to a fill depth of approximately 0.7 cm. The balance was placed on the middle shelf of a Christ Delta 1-24 KD laboratory-scale freeze-dryer of total shelf area 0.31 m^2. This machine contains three round shelves heated or cooled with silicone oil that are mounted under a cylindrical plexiglas cover completely encased in Al foil to reduce radiation heat transfer. The test vial to be measured was then placed within the holding arm of the balance. As required, further filled vials (10, 40 or 90) were placed around the balance plus test vial as illustrated in Fig. 1a. Observe

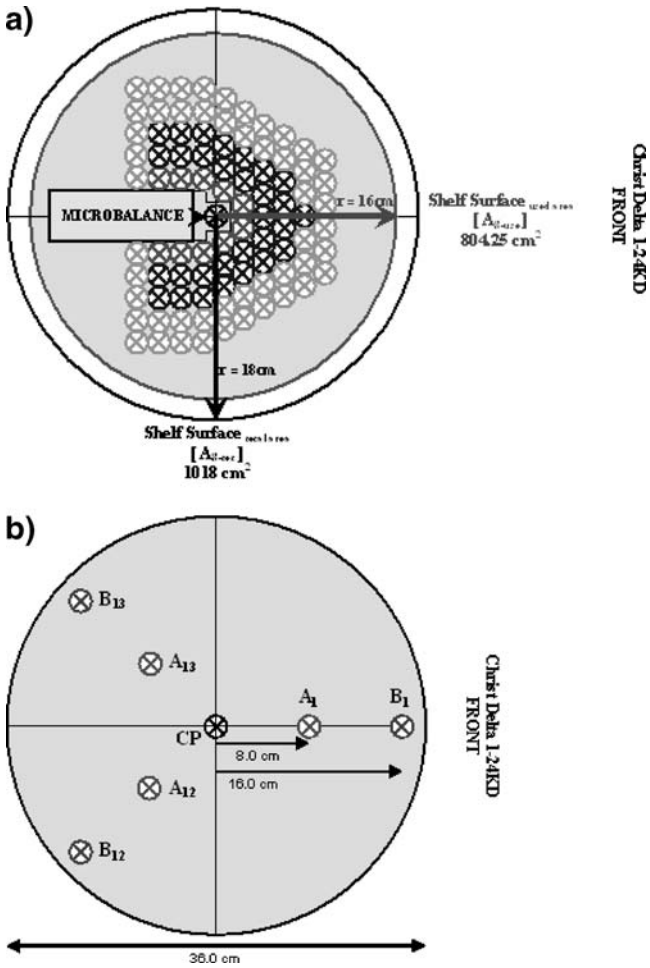

Fig. 1. **a** Packing of vials and balance on round shelf of the Christ freeze-dryer. The test vial placed in the geometric centre of the shelf was surrounded by either 10, 40 or 90 filled vials. **b** Position of single, non-surrounded vial to determine effect of shelf position on 1° drying time.

Table I. Freeze-drying Process Cycle Used for All Systems

Step	Shelf Temperature					
	Onset [°C]	End [°C]	Hold [min]	Ramp [°C/min]	Chamber Vacuum [mTorr]	Time [min]
1	+10	−40	–	1.67	–	30
2	−40	−40	90	–	–	90
3	−40	−24	–	0.13	25	120
4	−24	−24	1,440		25	1,440
5	−24	+24	–	0.09	10	560
6	+24	+24	–	–	10	360

that the presence of the balance does not allow a complete hexagonal close packing of vials which is standard in industrial freeze-drying because of maximum shelf loading (8) and reproducible heat transfer. The vial arrangement was hexagonal only in front of the balance test vial (Fig. 1a). Behind the test vial the vial packing had to be cubic to accommodate the presence of the balance itself. Freeze-drying was then performed using the process cycle given in Table I. The low chamber pressure of 25 m Torr during 1° drying was chosen to minimize the contribution of K_g to K_r in Eq. 2. (Note that throughout this work we use units consistent with those routinely employed on laboratory and commercial freeze-drying equipment. The pressure unit used is thus Torr rather than Pascal. Recall that 100 m Torr equals 13.3 Pa). The low chamber pressure should therefore allow more sensitive measurement of the effects of radiation heat transfer, ie K_r, to the test vial. Each formulation was freeze-dried in three replicate experiments to provide some idea of inter-run variation.

Characterization Methods

The residual moisture content of the dried samples was determined by Karl-Fischer-Titration using a Mitsubishi moisture meter (CA-06) with a water vapourizer (VA-06). Samples of 20–200 mg were treated at 140°C and an initial titration rate of 0.10 mg water/min with a dry N_2 gas stream of 200 ml/min ($n = 3$). Mid-point glass transition temperatures, T_g, were determined using a Mettler Toledo DSC 822. 5–10 mg of powder was sealed in Al pans and examined at a heating/cooling rate of 10°C/min. Each sample was cycled twice through the region of the glass transition. Product surface and internal morphology was examined on an Amray 1810T scanning electron microscope (SEM). The powders were Au-sputtered with a Hummer JR unit for 1.5 min.

RESULTS AND DISCUSSION

The vial packing density, $\emptyset$, as originally proposed by Placek (9) delineates the fraction of a shelf surface occupied by vials within a distance $r_v/\pi\, r_v^2$, where r_v is the vial external radius. We define ϕ in terms of the entire shelf area, A_s, occupied by the vials of number N_v including the inter-vial spaces for hexagonal close packing:

$$\emptyset = \frac{N_v \cdot A_v}{A_s - A_{mb}} \tag{3}$$

A_s is reduced by the area occupied by the balance, A_{mb}. Table II gives the values of $\emptyset$ according to Eq. 3 for the surrounding vial numbers used in this work. Although a maximum total vial number, N_v^{max}, of 160 is predicted on the shelf, only 145 vials could be manually positioned on this shelf area. The overestimation of N_v^{max} when using Eq. 3 is caused by the area of cubic close packing of the vials behind the test vial (see Fig. 1a). For a ratio of cubic to hexagonally packed vials of 1: 1 we re-write Eq.3 as:

$$\emptyset_2 = N_v \frac{[(4r_v^2 + r_v^2\pi)/2]}{A_s - A_{mb}} \tag{4}$$

Equation 4 predicts a N_v^{max} of 144 on the shelf (Table II), in good agreement with the experimentally-determined number of 145. We therefore use $\emptyset_2$ for the remains of this study.

Preliminary experiments illustrate how the position of the balance plus a single, non-surrounded test vial ($\emptyset_2 = 0$) on the shelf influences the duration of 1° drying (Table III). The shelf edge-positions B1, B1-2 and B1-3 show longer drying times than the shelf centre-positions A1, A1-2 and A1-3, and also the geometrical centre-position, CP (cf. Fig. 1b). This result with a single vial is unexpected, since radiation heat transfer from the chamber wall is known to be independent of pressure and length under otherwise identical experimental conditions. The cause could be the difference in temperature between the shelf and chamber walls and the different 'view factors' for a vial in the various positions. The contribution of K_r to K_v should, however, be the same at all shelf positions of the single vial. K_g and K_c are expected to be constant under given process conditions. It appears therefore that non-uniform heat transfer occurs across the shelf, most likely as a result of differences in shelf thickness or heat fluid distribution. Such non-uniform heat transfer across a shelf has already been reported in laboratory and production scale freeze-driers (3). This type of non-uniformity in heat transfer will influence K_g and K_c. Note that this phenomenon must be

Table II. Values of Vial Packing Density, Ø, Calculated for the Various Vial Loadings of One Shelf of the Christ Freeze-dryer

Number of Surrounding Vials	Ø Eq. 3	$\emptyset_2$ Eq. 4
0	0	0
10	0.062	0.069
40	0.248	0.277
90	0.558	0.622
Maximum (number)	0.992 (160)	0.996 (144)

Table III. Integrated Drying Time, t', for Ice from a Single, Non-surround Vial ($\emptyset_2 = 0$) at Various Positions on Shelf of Christ Freeze Dryer (see Fig. 1b)

Position	t' [min/mg]
B1	6.1
B1-2	6.1
B1-3	6.0
A1	5.7
A1-2	5.6
A1-3	5.7
CP	5.7

t' is defined by Eq.14

distinguished from faster sublimation occurring at the periphery of shelves fully-packed with vials (3), sometimes called the "edge vial effect." Here, the edge vials face a hotter surface (i.e. chamber wall or door) than do the centre vials and receive extra heat transfer by radiation. This will affect K_r. Based on these results all further experiments reported here were performed using the shelf centre-position, CP.

Pure Water

Figure 2a shows representative plots of cumulative water loss, $m(t)$ in g, and its first derivative the momentary drying-rate, $\dot{m}(t)$ in mg/10 min, *versus* 1° drying time, t, for the four different $\emptyset_2$ (cf. Table II). The reproducibility of the $m(t)$ and $\dot{m}(t)$ curves for $n = 3$ was very good, and each set of three replicate curves showed close superimposition (not given, for clarity). The $m(t)$ profiles are in their mid sections close to linear, with a downwards curvature becoming more evident at higher $\emptyset_2$. In a vacuum $m(t)$ is predicted to increase linearly with t for the case of sublimation into a sink from a planar ice surface that recedes with a constant rate. The $m(t)$ profiles deviate, however, from this zero order model. The drying-rate plots, $\dot{m}(t)$, illustrate that at given $\emptyset_2$ the sublimation rate changes during 1° drying and also that the end point of 1° drying is shifted to later times with higher $\emptyset_2$. It is also evident from Fig. 2a that increasing $\emptyset_2$ reduces $\dot{m}(t)$. For the case of sublimation of pure ice there is no dried-product layer being formed. We calculate therefore the residual ice-layer thickness, $L_{ice}(t)$ for a plane, receding sublimation interface from the values of $m(t)$:

$$L_{ice}(t) = \frac{m(\infty) - m(t)}{\rho A_p \varepsilon} \tag{5}$$

where ρ is the density of ice (we take this at the shelf-temperature, T_s (10)) and ε is its volume fraction in the formulation (=1.0). Equation 5 assumes that the ice surface remains planar and recedes normal to the vial's vertical axis during sublimation (6), to be discussed later. Figure 2b shows $\dot{m}(t)$ plotted *versus* $L_{ice}(t)$ for each $\emptyset_2$—note that $L_{ice}(t)$ decreases during 1° drying and moves therefore on the x-axis from right to left. The four plots all have the same shape independent of $\emptyset_2$, with $\dot{m}(t)$ shifted to lower values at higher $\emptyset_2$. The change from $\emptyset_2 = 0$ to $\emptyset_2 = 0.069$ greatly reduces $\dot{m}(t)$, but further increase to 0.277 and 0.622 only marginally reduces $\dot{m}(t)$ further. At constant T_s the $\emptyset_2$ will not alter either K_c or K_g in Eq. 2, and we expect only K_r to be reduced. In this case, Fig. 2b shows that a single layer of surrounding vials ($\emptyset_2 = 0.069$) strongly reduces radiation heat transfer radially through the test-vial wall to the sublimation front. The additional layers of surrounding vials at higher $\emptyset_2$ still have an effect on $\dot{m}(t)$, but it is much weaker. Indeed, the almost halving of $\dot{m}(t)$ when $\emptyset_2$ is increased from 0 to 0.069 (a single layer) means that the rate of radiation heat transfer to a single, non-surrounded vial, K_r, must be of similar magnitude to the rates of heat transfer through the vial base, i.e. $K_c + K_g$, under the process conditions ($P_c = 25$ m Torr) used.

$\dot{m}(t)$ initially increases rapidly up to a maximum value, denoted $\dot{m}_{max}$, before declining sharply to a plateau level at $L_{ice}(t) =$ approximately 6 mm. Subsequently $\dot{m}(t)$ decreases linearly until $L_{ice}(t) < 2.0$ mm, after which it falls rapidly to zero. This is the end point of 1° drying under the freeze-drying process conditions used here. The free sublimation rate of pure ice at a sublimation front temperature T_{ice} and

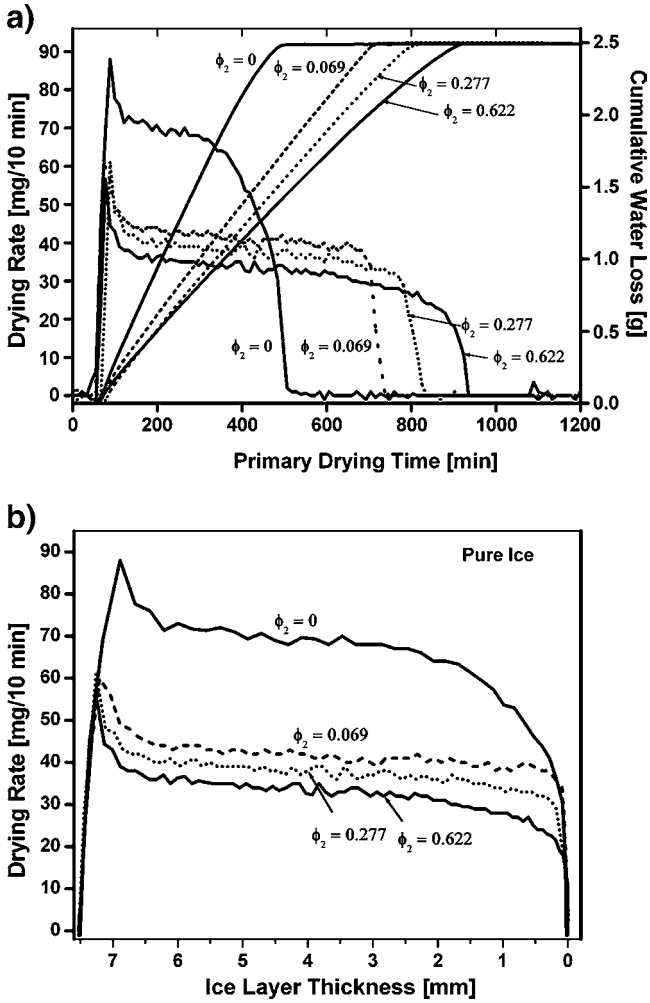

Fig. 2. Drying rate profiles for pure water. **a** Cumulative water loss, $m(t)$, *versus* process time, t, and $\sqrt{t}$. **b** Momentary drying rate, $\dot{m}(t)$, *versus* ice layer thickness, $L_{ice}(t)$ calculated from Eq. 5. Profiles determined at differing vial packing density, $\emptyset_2$.

chamber pressure P_c (μm Hg) can be estimated from kinetic theory by (10):

$$\dot{m}(t)\left[\mathrm{g/s\cdot cm^2}\right] = 4.375\times10^{-5}P_c\sqrt{\frac{M}{T_{ice}}} \quad (6)$$

where M is the solvent's molecular weight. As an estimate, $T_{ice} = -56°C$ for a T_s of $-25°C$ and P_c of 25 m Torr (4) during 1° drying (cf. Table I), Eq. 6 predicts a theoretical $\dot{m}(t)$ of >200 mg/10 min. Even for just the single, non-surrounded vial in Fig. 2b ($\emptyset_2 = 0$) the measured $\dot{m}(t)$ is much lower than this predicted value. Equation 6 is, however, a simple model that gives $\dot{m}(t)$ at a fixed T_{ice} and does not take into account non-steady state heat transfer conditions or an evapouration coefficient < unity. The lower measured values of $\dot{m}(t)$ must still in part be a result of insufficient heat-transfer to the sublimation front via all three pathways (K_c, K_g and K_r) to allow unhindered sublimation (11). The initial sharp $\dot{m}_{max}$ is evidently caused by over-shooting of the sublimation rate under the conditions prevailing at the sublimation front. The magnitude of this over-shoot, denoted $\dot{m}_{max}$, is the same at each $\emptyset_2$, i.e. approximately 15 mg/10 min. We suggest three possible causes for this over-shoot. First, that non-equilibrium conditions exist in the ice layer. At the beginning of 1° drying both T_s and P_c are ramped in parallel to their new settings, as is usual with this make of machine. It takes just a few minutes to reach the new value of P_c, whereas almost 3 1/2 h elapses before the new T_s is attained. The values of T_{ice} and P_c at the sublimation front may therefore show different lag phases followed by over-shoot of $\dot{m}(t)$ before reaching equilibrium. Secondly, although less likely, the ice of the surface layer may be more easily sublimed than that of the bulk ice formed during the freezing step with no air contact. In this case the surface ice layer could flash-off to cause over-shoot to $\dot{m}_{max}$, followed by a decrease to its equilibrium value determined by T_{ice} and P_c. Thirdly, it was observed that the condenser warms up by about 5°C as the initial load of water vapour freezes on it. This could reduce the driving force for sublimation and therefore depress $\dot{m}(t)$ after its initial peak at $\dot{m}_{max}$. We note that the condenser temperature did not change further during the latter course of 1° drying, indicating that the condenser's ice capacity was sufficient, even at the highest $\emptyset_2$ examined.

The linear decrease in $\dot{m}(t)$ with time at $6 \le L_{ice}(t) \le 2$ shows the same slope at each $\emptyset_2$. Since no dried-product layer is being formed, this decrease in $\dot{m}(t)$ may be a result of increasing path-length for the water molecules from the receding sublimation front through the air layer in the vial. $\dot{m}(t)$ will depend inversely on the total, momentary sublimation resistance of the vial's contents, $R_p(t)$:

$$\dot{m}(t) = \frac{P_0 - P_c}{R_p(t) + R_s} \quad (7)$$

where P_0 and P_c are the water vapour pressures at the sublimation interface and in the chamber, respectively, and R_s is the stopper resistance (=0 in the present study) (4). Pikal *et al.* (6) found that $R_p(t)$ of pure subliming ice in a glass capillary could be represented by:

$$R_{p(}t) = A_0 + A_1 l(t) \quad (8)$$

where $l(t)$ is the increasing air layer thickness, A_0 is a constant representing phase change resistance at the sublimation front, and A_1 represents the capillary tube, i.e. air layer, resistance. These authors found that an increase in chamber pressure increased both A_1 and A_0, as caused by more water/air inter-molecular collisions. Re-writing Eq. 8 in terms of $\dot{m}(t)$ and $L_{ice}(t)$ yields:

$$\dot{m}(t) = A_0' + A_1'[l_{air}^0 + L_{ice}(0) - L_{ice}(t)] \quad (9)$$

where A_0' and A_1' are constants representing the ease of the ice/vapour phase change and the permittivity of the air layer in the vial, and l_{air}^0 is the initial thickness of the air layer. A_0' and A_1' are given in Fig. 2b by the *y*-axis intercept of the extrapolated linear section of the plot of $\dot{m}(t)$ *versus* $L_{ice}(t)$, and its slope, respectively. Whereas A_0' is visually the same at each $\emptyset_2$, A_0' is smaller at higher $\emptyset_2$. The constancy of A_1' is expected, since air pressure in the vial is constant. In this case the observed decrease in $\dot{m}(t)$ in this phase can be attributed to increasing path length through the vial (air layer thickness $= l_{air}^0 + L(0) - L(t)$) and the associated increasing frequency of collisions (7) between the water and air molecules. A_1' will not be influenced by the presence of surrounding vials, i.e. the value of $\emptyset_2$, as indeed observed. It is, however, somewhat surprising that the larger air path length within the vial can have such a measurable impact on $\dot{m}(t)$. The alternative explanation for A_1' is that contact of the ice layer to the vial's sides and base is progressively lost during 1° drying, causing $\dot{m}(t)$ to decrease. Indeed, we observed the formation of a conically-shaped sublimation front with $\emptyset_2 = 0$, evidently caused by the substantial radiation heat transfer to the test vial's radial wall. The air layer between the vial side wall and the lateral face of the sublimation front will reduce heat transfer and lower $\dot{m}(t)$. Shrinkage of the ice layer away from the vial wall should be reduced, however, at higher $\emptyset_2$ because of the shielding effect of the surrounding vials. Yet we observe that A_1' is independent of $\emptyset_2$ making this alternative explanation unlikely. The decrease in $A_0'$with higher $\emptyset_2$ (Fig. 2b) is a result of hindered radiation heat transfer radially through the test-vial wall to the sublimation front, i.e. reduced K_r in Eq. 2. At $\emptyset_2 \ge 0.069$ the conical sublimation front was visibly much less obvious because of greatly reduced radiation heat transfer radially. A_1' remains unchanged.

Aqueous Mannitol Solution

Figure 3a shows the plots of $m(t)$ *versus* 1° drying time for the same $\emptyset_2$ used above with pure water. These profiles are clearly curved, much more so than the close-to-linear profiles seen with pure ice (cf. Fig. 2a). The end-point of 1° drying at the intersection with the *x*-axis is greatly extended when $\emptyset_2$ is larger. For the case of sublimation from a frozen solution contained in a vial into a vacuum sink with a planar sublimation front of area A that recedes through the dried-product layer, $m(t)$ should show a $\sqrt{t}$ relation of the sort (12): $m(t) = k\cdot m_0\cdot\varepsilon\cdot A\sqrt{t}$. Here, k is a constant, m_0 is the total mass of the frozen solution at $t = 0$, and ε is the volume fraction of ice in the solution. This is valid as long as the dried-product layer between sublimation front and solid top surface has a uniform resistance to water vapour flow, i.e. a

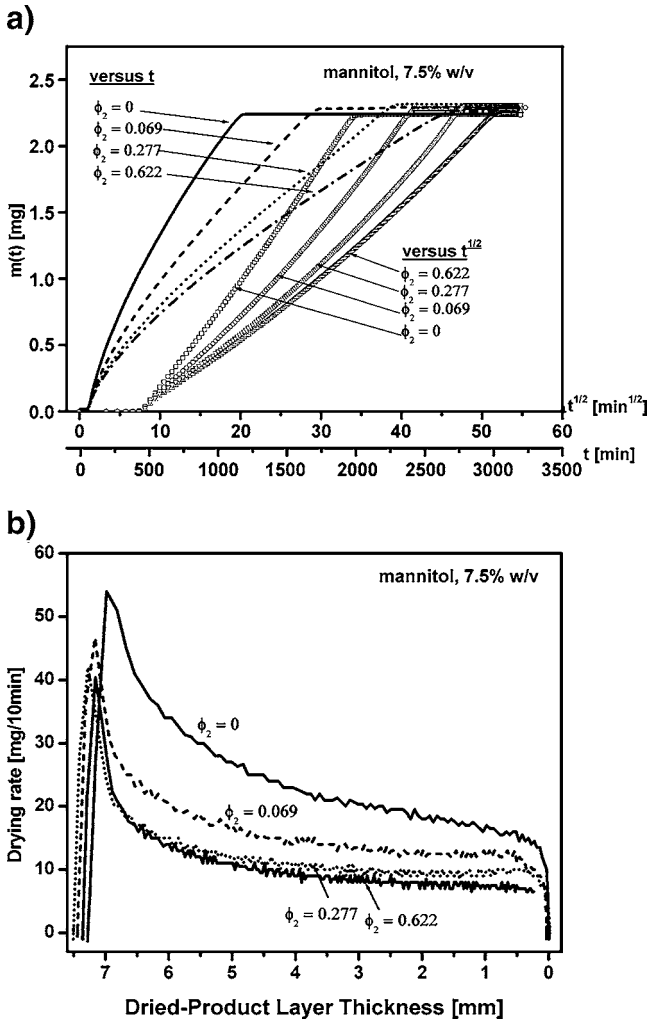

Fig. 3. Drying rate profiles for 7.5% w/v aqueous mannitol. **a** Cumulative water loss, $m(t)$, *versus* process time, t, and $\sqrt{t}$. **b** Momentary drying rate, $\dot{m}(t)$, *versus* dried-layer thickness, $l(t)$ calculated from Eq. 10. Profiles determined at differing vial packing density, $\emptyset_2$.

homogeneous internal structure. It also requires that heat transfer to the sublimation front is sufficient to maintain there a constant T_s and P_0. The plots of $m(t)$ *versus* $\sqrt{t}$ shown in Fig. 3a all show an upward curvature and hence an increasingly positive departure during 1° drying from the $\sqrt{t}$ model. There are a number of possible causes for this failure to observe the $\sqrt{t}$ model. First, at $\emptyset_2 = 0$ a comparison with the result for pure ice makes it appear likely that a conical sublimation front is formed within the frozen cake, although, clearly, this was not observable within the solid. In this case the enhanced area of the sublimation front would increase $\dot{m}(t)$ over that expected at a linear front. This will partly be compensated by reduced heat transfer through the lateral side of the cake through a layer of dried-product. In the presence of surrounding vials (i.e. $\emptyset_2 \geq 0.069$) we anticipate a more linear sublimation front, as observed with pure ice; yet the curvature of the $m(t)$ *versus* $\sqrt{t}$ plots is the same as at $\emptyset_2 = 0$. Secondly, the product temperature will certainly rise during 1° drying. One of the conditions of $\sqrt{t}$-behaviour—constant T_s—is therefore not being fulfilled. This will lead to a progressive increase in $\dot{m}(t)$—provided the vicinity of T_c is not reached—and hence a positive departure from the $\sqrt{t}$-model. Thirdly, the local product sublimation resistance becomes less as the path length within the dried-product layer increases. This would be the case for a crystalline mannitol matrix if the pore size is larger in the deeper regions of the dried-product layer. Yet when viewed under SEM (Fig. 4a) the structures of both the higher and deeper regions of the final cake appear homogeneous with a uniform ice ghost size. In this case of a largely homogeneous dried-product layer structure, the upwards drifting T_p appears the most likely cause of deviation from the $\sqrt{t}$ model for mannitol.

The profiles of $\dot{m}(t)$ in Fig. 3b reveal the details of how $\dot{m}(t)$ changes during 1° drying. The curve shape is different from that of Fig. 2b for pure water. Note that in contrast to the pure ice, we now use the dried-product layer thickness, $l(t)$, for the solutions examined (7):

$$l(t) = \frac{m(0) - m(t)}{\rho A_p \varepsilon} \tag{10}$$

For the single, non-surrounded vial ($\emptyset_2 = 0$) $\dot{m}_{max}$ is followed by a sharp decline in $\dot{m}(t)$ concave to the x-axis over the complete range $6.5 \leq l(t) \leq 0.5$, and not linear as with pure ice (cf. Fig. 2b). This sharp, continual decline in $\dot{m}(t)$ reflects the increasing total resistance of the dry-product layer to water vapour transport, $R_p(t)$ as in Eq. 7. The cause is an increasing path-length for the water vapour between the receding sublimation front and the dried-product layer's top surface. The strongly concave profiles in Fig. 3b (at all $\emptyset_2$s) are equivalent to the type IV product resistance behaviour identified by Pikal *et al.* (7) for crystalline KCl from glass capillary experiments. These authors attributed non-linearity of $R_p(t)$ *versus* $l(t)$ to variation in dried-product layer structure as $l(t)$ increases. The curvature in Fig. 3b is, however, quite close to the behaviour expected for a homogeneous structure, where the plots of $m(t)$ *versus* $\sqrt{t}$ in Fig. 3a are only marginally curved because of upwards drift in T_s. The total resistance of the dry-product layer, $R_p(t)$, increases with greater $l(t)$:

$$R_p(t) = l(t) \cdot R^* \tag{11}$$

R^* is the local resistance of the dried-product layer per unit length, which will be constant throughout the dried-product layer in the case of a homogeneous morphology. The solution of Eq. 7 and 11 will be (near-) linear $m(t)$ *versus* $\sqrt{t}$ behaviour observed with mannitol. Additionally, the dried-product's top surface (Fig. 4b) shows a different structure from that of the bulk cake. The formation of this surface region at the onset of 1° drying is evidently responsible for the much lower $\dot{m}_{max}$ reached with mannitol (45 mg/10 min) than that seen with pure ice (89 mg/10 min) at the same $\emptyset_2 = 0$. Pikal *et al.* (7) attributed non-zero values of $R_p(0)$ to the resistance offered by formation of a surface structure. We expect therefore that this surface structure will hinder the further passage of water vapour passing up through the underlying dried-product layer. The effect of this on $\dot{m}(t)$ behaviour will be to introduce a surface resistance, R_s, that is

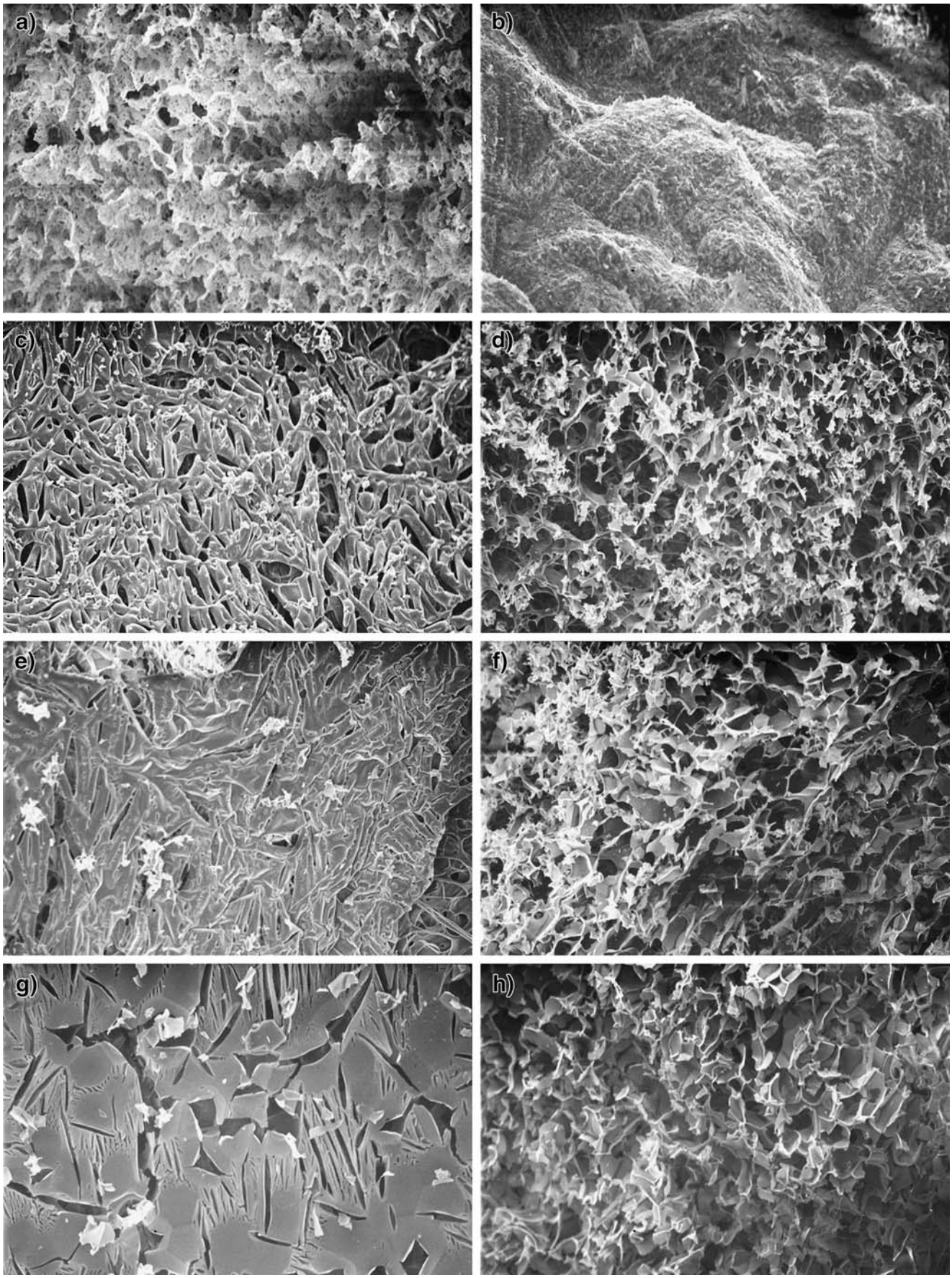
a)
b)
c)
d)
e)
f)
g)
h)

◀ **Fig. 4.** Scanning electron micrograph images of various dried products. **a** mannitol inside cake; **b** mannitol top surface; **c** sucrose top surface; **d** sucrose inside cake; **e** trehalose top surface; **f** BSA top surface; **g** trehalose inside cake; **h** BSA inside cake.

a constant part of the increasing total resistance of the dried-product layer to water vapour transport, $R_p(t)$:

$$R_p(t) = R_s + l(t)R^* \tag{12}$$

$\dot{m}(t)$ will show a $\dot{m}_{max}$ depending on the value of R_s. The subsequent goodness of fit to $\sqrt{t}$ behaviour is then determined by the homogeneous internal morphology of the crystalline mannitol cake overlayed by the upwards drift in T_s during 1° drying. This implies from Eq. 12 that $R_s < l(t)R^*$ and does not represent the major barrier to water vapour transport in the vial.

Increase in vial load from $\emptyset_2 = 0$ up to $\emptyset_2 = 0.622$ maintains the same, concave drying-rate profile, which is, however, shifted to lower values of $\dot{m}(t)$ (Fig. 3b). As seen in Fig. 2b with pure ice, a single layer of vials ($\emptyset_2 = 0.069$) substantially reduces $\dot{m}(t)$, whereas further increase in $\emptyset_2$ has much less effect on $\dot{m}(t)$. In this case a dried-product layer is being formed, yet K_r still plays a major role in heat transfer to the single, non-surrounded vial. This role is greatly reduced when surrounding vials are present. Neither the lower $\dot{m}(t)$ nor the higher T_p caused by the shielding-effect of the surrounding vials has evidently any influence on profile shape and hence homogeneous cake structure. We emphasize that the low chamber pressure used in this study (25 m Torr) will magnify the influence of vial load ($\emptyset_2$) on drying behaviour, as we wished to examine the 'worse case'. More conventional drying conditions will certainly show a moderated effect of $\emptyset_2$ on $\dot{m}(t)$.

Aqueous Sucrose Solution

The drying rate profile of $\dot{m}(t)$ *versus* $l(t)$ with $\emptyset_2 = 0$ shown in Fig. 5b is quite different from that seen in Fig. 3b for mannitol. The initial peak at $\dot{m}_{max}$ of approximately 60 mg/10 min is higher than that seen with mannitol and does not fall-off so sharply as sublimation proceeds. Indeed, the plot of $\dot{m}(t)$ decreases convex to the *x*-axis. It follows that the total resistance of the dried-product layer, $R_p(t)$, increases much less rapidly with $l(t)$ than expected for a homogeneous cake (cf. the sharply concave mannitol profile). The strongly curved profiles of $m(t)$ *versus* $\sqrt{t}$ shown in Fig. 5a can be attributed to upwards drift in T_s during 1° drying, as seen with mannitol. The shape of the $\dot{m}(t)$ plots suggests, however, heterogeneous internal cake structure and an R^* in Eq. 11 that is not constant.

As mentioned above, Pikal *et al.* (7) attributed all non-linear profiles of $R_p(t)$ *versus* $l(t)$ to variation in dried-product layer internal structure as $l(t)$ increases. The convex profile to the *x*-axis seen in Fig. 5b for sucrose was, however, not shown by any of the crystalline or amorphous products reported by these authors. According to Eq. 12 this maintenance of a high $\dot{m}(t)$ over a prolonged part of 1° drying means that R^* decreases from the top to the bottom of the dried-layer. This would be the case if the pore size becomes larger when moving from the top into the deeper regions of the cake. Consequently, $\dot{m}(t)$ remains high as $l(t)$ increases and then falls off sharply at the end of 1° drying. Such heterogeneity could be a result of micro-collapse of the mechanically-flexible, amorphous sucrose structure causing formation of large combined pores. Additionally, shrinkage and detachment of the amorphous cake from the inside vial wall—as known for sucrose formulations (13)—would expose the cylindrical side walls of the cake and allow enhanced water vapour loss. Both of these mechanical changes would be expected to be more pronounced with the amorphous sucrose than with the crystalline mannitol. The SEMs of internal dried-product morphology of the sucrose reveal no clear evidence of collapse as the source of heterogeneity (e.g. Fig. 4d). Additionally, the formation of a conical sublimation front expected to occur at $\emptyset_2 = 0$ may lead to heterogeneous behaviour. Whatever the explanation, heterogeneity of the internal cake structure renders R^* in Eq. 12 no longer constant, but rather a function of $l(t)$:

$$R_p(t) = R_s + l(t) \cdot R^*(l(t)) \tag{13}$$

The nature of the relation $R^* = f(l(t))$ will now determine the $\dot{m}(t)$ profile, providing R_s—the resistance of the surface

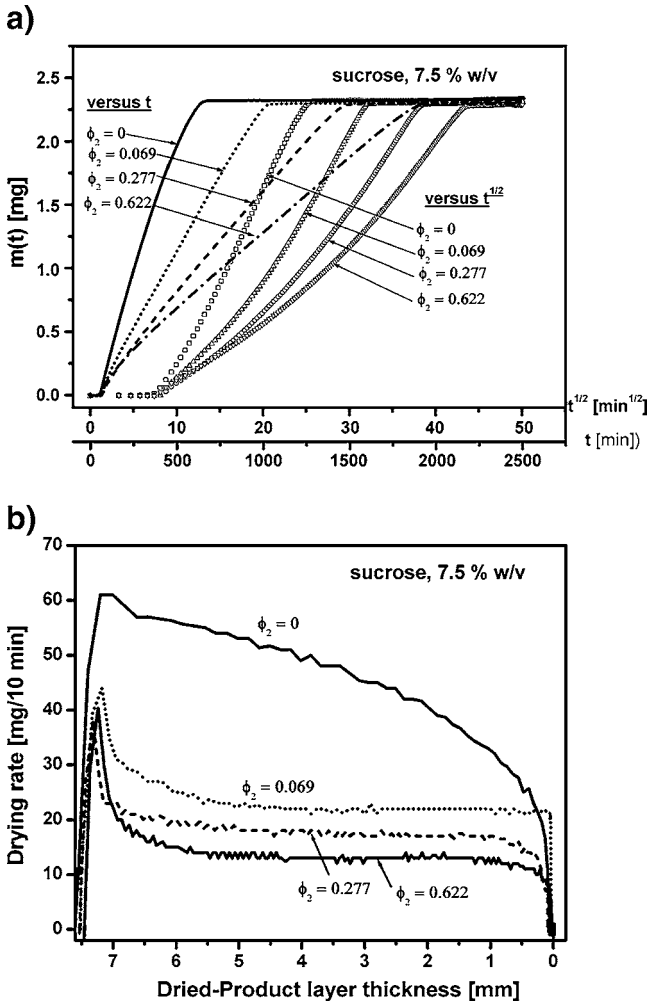

Fig. 5. Drying rate profiles for 7.5% w/v aqueous sucrose. **a** Cumulative water loss, $m(t)$, *versus* process time, t, and $\sqrt{t}$. **b** Momentary drying rate, $\dot{m}(t)$, *versus* dried-layer thickness, $l(t)$ calculated from Eq. 10. Profiles determined at differing vial packing density, $\emptyset_2$.

structure—is not rate-limiting. If $R_s \geq l(t)R^*$ in Eq. 12, then $R_p(t) \rightarrow R_s$ and the drying rate through a high-resistance surface structure will tend to constancy. The solution of Eq. 12 and 7 will now be: $\dot{m}(t) = kt$. Fig. 5b shows indeed how for $\emptyset_2 = 0$ the measured $\dot{m}(t)$ is flat and shows only a slow decline with increasing $l(t)$. The sucrose dried-product's top surface (Fig. 4c) shows, however, a filament-like structure that appears to be less dense than the top surface of the mannitol (cf. Fig. 4b). Indeed, $\dot{m}_{max}$ is higher with sucrose (60 mg/10 min) than with mannitol (45 mg/10 min) thus correlating well with observed surface structure.

The $\dot{m}(t)$ profile is changed in the presence of surrounding vials (Fig. 5b). After $\dot{m}_{max}$ the profiles decline strongly concave to the *x*-axis up to $l(t) \approx 6$ mm, and then show a lengthy plateau phase of constant $\dot{m}(t)$ extending across the range 6 mm $\leq l(t) \leq 1$ mm. As seen with both pure ice and mannitol, the surrounding vials reduce $\dot{m}(t)$ and $\dot{m}(t)$ substantially, evidently by hindering radial radiation heat transfer to the test-vial wall. In the case of the sucrose, however, the profile shape at early time is also altered by the presence of the surrounding vials. Either the lower $\dot{m}(t)$ or the higher T_p lead to this initial sharp decline in $\dot{m}(t)$ that is reminiscent of that seen with the homogeneous mannitol cake in Fig. 3b. The later flat plateau phase is still a clear indication that at later time the increasing $l(t)$ is not causing higher total dried-layer resistance, $R_p(t)$. The $\dot{m}(t)$ stays conspicuously constant in this plateau phase, whose length is independent of $\emptyset_2$. Although this behaviour is predicted by Eq. 13 for the case that $R_s >> l(t)R^*$ and water vapour passage through the skin is rate-limiting, the visibly porous skin structure in Fig. 4c is permeable (cf. its $\dot{m}_{max}$). The presence of surrounding vials thus alters heat transfer such that it produces change in cake heterogeneous structure resulting in altered $\dot{m}(t)$ profile.

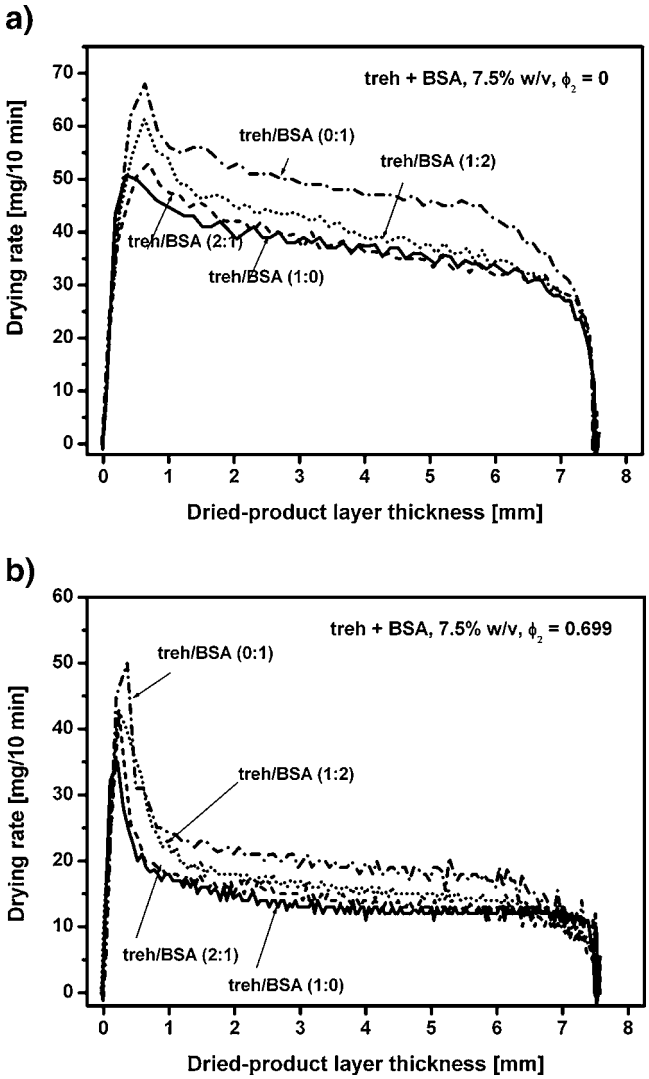

Fig. 6. Drying rate profiles for various 7.5% w/v aqueous trehalose/BSA binary mixtures. **a** $\emptyset_2 = 0$. Momentary drying rate, $\dot{m}(t)$, *versus* dried-layer thickness, $l(t)$. **b** $\emptyset_2 = 0.622$. Momentary drying rate, $\dot{m}(t)$, *versus* dried-product layer thickness, $l(t)$.

Aqueous Trehalose/BSA Solution

The $m(t)$ *versus* t profiles obtained for aqueous solutions of either trehalose or BSA (not shown for brevity) are qualitatively the same as seen for sucrose. Consequently the plots of $m(t)$ *versus* $\sqrt{t}$ are non-linear, being upward curved indicating most likely an upwards drift in T_s. Quantitative differences are evident in the drying rate profiles shown for various trehalose/BSA mixtures at $\emptyset_2 = 0$ and $\emptyset_2 = 0.699$ in Fig. 6a and b, respectively. At $\emptyset_2 = 0$, $\dot{m}_{max}$ for the pure trehalose is 50 mg/10 min, which is lower than that of 60 mg/10 min seen with sucrose. The surface structure in Fig. 4e has more closely packed filaments than that seen with sucrose in Fig. 4c. Increasing proportion of BSA in the trehalose/BSA mixtures leads to higher $\dot{m}_{max}$, reaching almost 70 mg/10 min with pure BSA (Fig. 6a). The surface structure with the pure protein (Fig. 4f) indeed shows large fissures in a smooth surface than can account for the high $\dot{m}_{max}$. For all of the solutions investigated here the measured value of $\dot{m}_{max}$ relates therefore well to surface structure appearance under SEM. This provides some justification for including R_s in Eq. 12 and 7 as a constant part of $R_p(t)$. The $\dot{m}(t)$ profiles of pure trehalose, pure BSA as well as all of their mixtures at $\emptyset_2 = 0$ (Fig. 6a) show how $\dot{m}(t)$ decreases after $\dot{m}_{max}$ linearly in the range $2 \leq l(t) \leq 6$ mm. These profiles are not convex to the *x*-axis, as seen with pure sucrose. Accepting that the surface structure is not rate-limiting, this means that in these two pure materials and their mixtures the heterogeneous dried-product layer morphology is extenuated. This draws the $\dot{m}(t)$ profile partly down towards the behaviour of a homogeneous internal morphology (cf. mannitol in Fig. 3b). There are no obvious reasons for the different drying behaviour of the two carbohydrates sucrose and trehalose, which is somewhat surprising. Furthermore, the drying rate profiles of the single, non-surrounded vial in Fig. 6a show that the trehalose dries more slowly than the sucrose. The addition of the protein accelerates drying.

The presence of surrounding vials—even just a single layer with $\emptyset_2 = 0.069$—results in the same dramatic alteration in $\dot{m}(t)$ profiles at early time to strongly concave to the *x*-axis (Fig. 6b) as seen with sucrose. After $\dot{m}_{max}$ the $\dot{m}(t)$ profiles decline sharply to an extended plateau phase. Again, we interpret this change in profile shape to reduced heterogeneity caused by the lower $\dot{m}(t)$ and hence higher T_p in the presence of the surrounding vials.

Relation Between Primary Drying Time and $\emptyset_2$

To quantify the duration of 1° drying when using the balance we define an integrated 1° drying time, t', in min mg^{-1} that utilizes all of the measuring points on the $\dot{m}(t)$ *versus* t curve:

$$t' = \frac{t_{pd}}{AUC_{0\rightarrow t_{pd}}} \tag{14}$$

$AUC_{0\rightarrow t_{pd}}$ (in mg) is equal to the total amount of sublimed ice up to constant balance weight. It is calculated from the measured $\dot{m}(t)$ in each time unit, Δt, of 10 min, t_n:

$$AUC_{0\rightarrow t_{pd}} = \sum_n \dot{m}\,(t_n)\cdot \Delta t_n \tag{15}$$

t_{pd} in min is the graphically-determined end-point of 1° drying, which we take to be where $\dot{m}(t)$ reaches ≤ 0 mg/10 min for two consecutive time points. Fig. 7a shows how t' increases with higher vial packing density for all of the pure substances examined. With the exception of water, each plot of $t'(\emptyset)$ *versus* $\emptyset_2$ can be represented empirically as a power

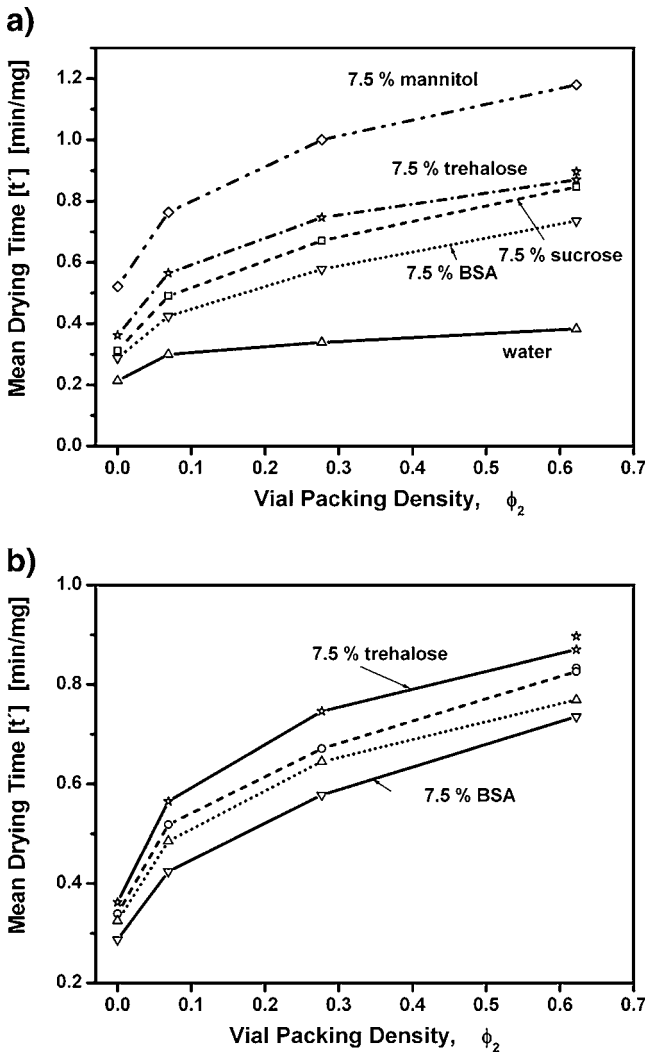

Fig. 7. Dependence of integrated drying time, t', on $\emptyset_2$. **a** Pure materials. **b** Binary mixtures of trehalose plus BSA. t' is calculated from Eq. 14.

Table IV. Fitting of the Function: $t'(\emptyset) = t_0' + c\emptyset_2^n$ to Data from Fig. 7a and b

Formulation	t_0' [min/mg]	c [min/mg]	n
Mannitol	0.52	0.82	0.44
Sucrose	0.31	0.68	0.50
Trehalose	0.36	0.62	0.40
BSA	0.29	0.56	0.54
Tre/BSA (2:1)	0.34	0.60	0.46
Tre/BSA (1: 2)	0.33	0.58	0.45

The values for water did not fit to this equation and could be better represented by a straight line.

relation of the form: $t'(\emptyset_2) = t_0' + c\emptyset_2^n$, where t_0' is the value measured for a non-surrounded vial ($\emptyset_2 = 0$), and c and n are constants representing magnitude (i.e. drying rate) and curvature (i.e. influence of $\emptyset_2$), respectively. The values obtained for c and n from a non-linear, least-squares fitting of this function to the $t'(\emptyset)$ data in Fig. 7a are given in Table IV. Only water does not fit to this function. The protein dries the fastest at all $\emptyset_2$, as is reflected in the lowest value for c, followed by sucrose and then the trehalose. The slowest to dry is the crystalline mannitol under the process conditions examined here (which, of course, are not typical for this substance). The fitted values of n are broadly similar, lying between 0.4 and 0.54. The shielding effect of surrounding vials on sublimation rate of the test vial is therefore substance unspecific. The influence of the surrounding vials on radiation heat transfer is, clearly, exerted outside the vial.

The residual moisture contents of both disaccharides at the end of freeze-drying increase with higher $\emptyset_2$, as shown in Table V. Accordingly the T_g values decrease at higher $\emptyset_2$. The reduction in radiation heat transfer radially to the test vial caused by the presence of the surrounding vials therefore not only decreases momentary $\dot{m}(t)$ but also reduces the total amount of water removed up to the end of the complete drying cycle. This cannot be a result of insufficient time for completion of 1° drying, since $\dot{m}(t)$ always reached zero well within the programmed duration of 1° drying (e.g. see Fig. 3a for mannitol). This surprising result means that the presence of surrounding vials influences the equilibrium moisture content of the test vial at the end of freeze-drying. Additionally, the faster-drying sucrose has a higher end residual moisture content than does the slower-drying trehalose (Table V). The sorption isotherms of these two amorphous disaccharides indeed show a higher equilibrium moisture content of the sucrose under given conditions of air temperature and relative humidity (14,15).

Table V. Residual Moisture Contents and Glass Transition Temperatures, T_g, Determined in Dried Products

System	$\emptyset_2$	Residual Water [% w/v]	T_g [°C]
Sucrose	0	0.70	64.4
	0.069	0.73	63.7
	0.277	0.83	62.2
	0.622	0.84	61.6
Trehalose	0	0.52	110.0
	0.069	0.60	107.6
	0.277	0.69	108.0
	0.622	0.76	101.9

The addition of BSA to the trehalose reduces t' across all values of $\emptyset_2$ (Fig. 7b). The fitted values of c decrease steadily with increasing fraction of protein in the trehalose/BSA binary mixtures (Table IV). The higher drying rate of the protein cannot be related to differences in internal dried-layer morphology, which under SEM is seen to be similar for trehalose (Fig. 4g) and BSA (Fig. 4h).

CONCLUSIONS

1) Plots of momentary drying rate *versus* residual layer thickness for pure ice in a standard vial yielded the constants representing the ease of the ice/vapour phase change and the permittivity of the air layer in the vial.
2) A crystalline mannitol cake in a non-surrounded vial shows a temporal drying rate profile that is indicative of a largely homogeneous dried-product layer internal morphology. In the presence of surrounding vials the reduced heat transfer to the test vial from the walls of the freeze dryer chamber results in a substantial reduction in drying rate, but no effects on cake morphology are seen.
3) The temporal drying rate profile of an amorphous sucrose cake in a non-surrounded vial can be explained by substantial heterogeneity in internal structure of the dried-product layer, owing possibly to shrinkage or microcollapse. The presence of surrounding vials evidently enhances steady state conditions and produces a shift in temporal drying rate profile towards that of a more homogenous cake structure.
4) The observable surface structure of the dried-product layers correlates to their initial maxima of drying rate. As a result this surface resistance should be considered as a constant part of total dried-product resistance.
5) Pure trehalose dries more slowly than pure sucrose. Its temporal drying rate profile is intermediate between those for mannitol and sucrose. The same is observed with the model protein BSA, whose addition to either disaccharide decreases primary drying time substantially.

ACKNOWLEDGEMENTS

We gratefully acknowledge the support of Martin Christ GmbH who provided the balance for performing this work.

REFERENCES

1. C. Roth, G. Winter, and G. Lee. Continuous measurement of drying rate of crystalline and amorphous systems during freeze-drying using an *in situ* microbalance technique. *J. Pharm. Sci* **90**:1345–1355 (2001).
2. C. Roth, G. Winter, and G. Lee. Novel microbalance technique for measuring drying rate during freeze-drying. *Proceed. 3rd World Meeting Pharm. Biopharm., Pharm. Technol.*, Berlin. (2000).
3. S. Rhambhatla, and M. J. Pikal. Heat and mass transfer scale-up issues during freeze-drying. I. Atypical radiation and edge vial effects. *AAPS. Pharm. Sci. Tech* **4**(2):111–120 (2003).
4. H. Costantino, and M. Pikal. Lyophilisation of Biopharmaceuticals. In: AAPS Press Series Biotechnology: Pharmaceutical Aspects, Vol. 2 (2005).
5. S. Rambhatla, S. Tchessalov, and M. J. Pikal. Heat and mass transfer scale-up issues during freeze-drying. III. Control an characterization of dryer differences via operational qualification tests. *AAPS Pharm. Sci. Tech*. **7**(2) Article 39 (2006).
6. M. J. Pikal, M. L. Roy, and S. Shah. Mass and heat transfer in vial freeze-drying of pharmaceuticals: role of the vial. *J. Pharm. Sci* **73**(9):1224–1237 (1984).
7. M. J. Pikal, S. Shah, D. Senior, and J. Lang. Physical chemistry of freeze-drying: measurement of sublimation rates for frozen aqueous solutions by a microbalance technique. *J. Pharm. Sci* **72**:635–650 (1983).
8. BOC Edwards Pharmceutical Systems, www.bocedwards.com.
9. J. Placek. *Heat transfer limitations, their reduction and control. Proceed. Freeze-Drying Pharm Biologic*, Breckenridge (2001).
10. S. Dushman, and M. Lafferty. *Scientific Foundations of Vacuum Technique*. Wiley, NY, 1962, pp. 1–73.
11. S. Nail, and L. Gathin. Freeze drying: principles and practice. In A. Lieberman, and L. Lachmann (eds.), *Pharmaceutical Dosage Forms, Vol. 2*, Marcel Dekker, NY, 1993, pp. 163–233.
12. J. Mellor. *Fundamentals of Freeze Drying*, Academic, NY, 1978.
13. S. Rambhatla, J. P. Obert, S. Luthra, C. Bhugra, and M. J. Pikal. Cake shrinkage during freeze drying: a combined experimental and theoretical study. *Pharm. Dev. Technol* **1**:33–40 (2005).
14. S. Shamblin and G. Zografi. The effects of absorbed water on the properties of amorphous mixtures containing sucrose. *Pharm. Res* **16**:1119–1124 (1999).
15. H. Iglesias, F. Chirife, and M. Buera. Adsorption isotherm of amorphous trehalose. *J. Sci. Food. Ag* **75**:183–186 (1997).